Theor Chem Acc (2012) 131:1200
DOI 10.1007/s00214-012-1200-4

REGULAR ARTICLE

# Geometries and stabilities of $Ag_n^v$ ($v = \pm1, 0$; $n = 21$–$29$) clusters

**Shu-Yao Yan · Wei Zhang · Zeng-Xia Zhao · Wen-Cai Lu · Hong-Xing Zhang**

Received: 21 August 2011 / Accepted: 27 February 2012 / Published online: 15 March 2012


**Abstract** We performed a systematical study on the lowest-energy structures of the medium-sized silver clusters $Ag_n$ ($n = 21$–$29$) by using a genetic algorithm coupled with a tight-binding method, and the DFT calculations with Perdew–Wang generalized-gradient approximation. The corresponding cluster ions were also searched based on the neutral cluster structures. It is found that the $Ag_{21-23}$ prefer icosahedron or double-icosahedron as core structures. $Ag_n$ ($n = 24$–$27$) favor a bulk-like fcc stacking motif. $Ag_{28}$ and $Ag_{29}$ tend to high symmetrical structures. The relative stabilities, the ionization potentials and electronic affinities of silver clusters analyzed in the paper are consistent with the experimental data. It is interesting to find that the experimental spectra fit reasonable well the optical absorption spectra obtained with the structures calculated by us.

**Keywords** Silver clusters · Density functional theory · Structures · Ionization potentials and electronic affinities · Absorption spectra

S.-Y. Yan · W. Zhang · Z.-X. Zhao · W.-C. Lu · H.-X. Zhang (✉)
State Key Laboratory of Theoretical and Computational Chemistry, Institute of Theoretical Chemistry, Jilin University, Changchun 130021, Jilin, People's Republic of China
e-mail: zhanghx@jlu.edu.cn

W.-C. Lu
College of Physics, Qingdao University, Qingdao, People's Republic of China

W.-C. Lu
Laboratory of Fiber Materials and Modern Textile, The Growing Base for State Key Laboratory, Qingdao University, Qingdao 266071, Shandong, People's Republic of China

## 1 Introduction

Coinage metal (Au, Ag, Cu) clusters and nanoparticles have been received a great deal of attention. Silver clusters are the focus of numerous investigations since they play important roles in photography, catalytic processes, novel electronic materials, surface science and metal alloy clusters [1–9]. It is well known that geometrical structures of clusters determine their special physical and chemical properties. In order to better understand unique properties, electronic and geometric structures of silver clusters are extensively studied experimentally and theoretically.

Experimental measurements and theoretical results from density functional and MP2 calculations of ion mobility suggested that cationic silver clusters $Ag_n^+$ have planar structures for $n = 3$–$4$ and form three-dimensional (3-D) structures at $n = 5$ [10]. However, Huda and Ray [11] advanced that the lowest-energy structures of $Ag_6$ and charged $Ag_7$ begin to show 3-D geometries. Similar results were obtained by Fournier [12], and they also reported that the most stable structures of neutral $Ag_n$ have prolate structures starting at $n = 10$. Meanwhile, Zhang and Tian [13] revealed that global minima of neutral and charged silver clusters adopt closed-flat double-layered geometries at the size from 9 to 14 atoms. In addition, experimental optical absorption spectra of $Ag_n$ ($n = 4$–$22$) coupled with DFT calculations from Harb et al. [14] indicated a structural transition from double-layered structures for $n = 12$–$16$ to quasispherical and compact arrangements for $n \geq 18$. A similar trend of structural evolution was reflected by computational optical absorption spectra for the intermediate-size silver clusters [15]. The most stable configuration of $Ag_{20}$ is a tetrahedral structure by Wang et al. [16]. In contrast, some recent studies revealed that silver clusters prefer to grow in an icosahedral pattern

around the size from 9 to 20 atoms [17–19]. Itoh et al. [20] optimized geometries of $Ag_n$ ($n = 2$–75) and explained that the structural types of the most stable structures change in the order for line → plane → open → closed with increasing cluster size. Most recently, the structural assignments of anionic clusters $Ag_{55}^-$ and $Ag_{57}^-$ were successfully investigated by applying photoelectron spectroscopy (PES) [21]. As to larger-sized clusters, a modified dynamic searching was carried out by Yang et al. [22] to search for global minima of silver clusters from 13 to 160 atoms. According to their study, the stable motif of $Ag_n$ transfers an icosahedron ($n = 49$–61) into a decahedron ($n = 62$–160).

In this work, a systematical investigation of the ground-state geometries, relative stabilities, ionization potentials, electronic affinities and optical absorption spectra of silver clusters with up to 29 atoms was performed. This paper is intended to explore the trend of structural evolution of $Ag_n$ ($n = 21$–29), which is still an uncertain issue in studies of silver clusters. Genetic algorithm (GA) and density functional theory (DFT) were used to investigate the lowest-energy geometries and isomers for medium-sized clusters $Ag_n$ ($n = 21$–29). For the neutral clusters, it is found that the ground states of $Ag_{21-23}$ are resulted from a 13-atom icosahedron or 19-atom double-icosahedron. We found that the lowest-energy structures of $Ag_n$ ($n = 24$–27) also have a tendency to pack in a bulk-like stacking pattern. Compared to the calculated binding energy per atom (2.647 eV) of bulk Ag (lattice constant $a_0 = 4.0857$ Å), the binding energies of these Ag clusters are about 0.576–0.613 eV smaller. The most stable isomers for $Ag_{28}$ and $Ag_{29}$ tend to high symmetrical structures. For cationic and anionic clusters, they behave a different structural growth from the neutral ones. In order to achieve a better understanding of silver clusters, we analyzed the properties of the silver clusters including binding energies per atom, second differences in energies and HOMO–LUMO gaps. As the means of evaluating electronic stability, we carried out a detailed study on the ionization potentials and electronic affinities of $Ag_4$–$Ag_{29}$ clusters. For further to assess our lowest-energy structures, we have calculated optical absorption spectra for the medium-sized clusters $Ag_n$ ($n = 21$–29). This paper is organized as follows. In Sect. 2, we present the computational methods and parameters used in this study. The results and discussion for the structures, relative stabilities, ionization potentials, electronic affinities and the optical absorption spectra are given in Sect. 3. Finally, Sect. 4 summarizes our main conclusions.

## 2 Methodology

The GA [23] coupled with a TB potential of silver was applied in this work to identify low-energy candidates of $Ag_n$ ($n = 21$–29) clusters. Environment-dependent TB potential model advanced by Zhang et al. [24, 25] was used to develop the TB silver potential. In our present work, the computational procedure is described as follows. Two parental structures A and B from the starting population produce offspring structures C and D by cutting A and B into two halves and permuting their lower halves. If the offspring structures have lower energies than parental structures, the parent will be replaced by lower-energy offspring to start next reproduction. And almost 200 TB energy evaluations are required for average structure in GA/TB research. Although GA/TB method is an important computational tool for finding isomers of clusters, the results of GA simulation may not include all possible competing structures due to the limitation of GA and silver TB potential. Therefore, we also added some handmade structures to pool to obtain more competing candidates. The lowest-energy structures of the $Ag_n$ ($n = 21$–29) cluster ions were also searched based on the corresponding neutral cluster structures.

In order to assess the stability, low-energy candidates were further investigated systematically by using the first principle calculations. The first principle calculation by DFT is nowadays one of the best methods to study small and medium-sized systems. All calculations in this study were performed within DFT framework implemented in $DMol^3$ included in materials studio (MS) [26, 27]. Perdew–Wang generalized-gradient approximation (PW91) [28] was used to describe exchange and correlation effects. Density functional semi-core pseudo-potential (DSPP) was used as the core treatment parameter. DSPP considers relativistic effects of core electrons as a simple potential, including some degree of relativistic correction into the core [29] and can be very useful approximations for heavier elements. The double numerical plus polarization function (DNP) was chosen as the basis set [26]. A global real space cutoff (0.3 eV/atom) was selected for generation of the numerical basis set. In order to achieve accurate electronic convergence, a smearing (0.005 hartree) to the orbital occupation and global orbital cutoff radius (4.0 Å) were applied in our calculations. The $k$-point grid was generated using a $k$-point separation (0.05 $Å^{-1}$) appropriate to the specified quality level. All structures in this study were relaxed until the convergence tolerance of energy reaches $1.0 \times 10^{-5}$ hartree. The convergence criteria and basis set used in this paper guarantee the accuracy of calculation results. We also calculated the relative energies for isomers of silver clusters $Ag_n$ ($n = 21$–29) at the TB and DFT levels, respectively. The TB energy differences differ from the DFT energy differences by 0.98 eV on average. And time-dependent DFT was employed to calculate the optical absorption spectra.

## 3 Results and discussion

### 3.1 Geometries and relative energies

Figures 1 and 2 present three low-energy isomers for neutral silver clusters and the lowest-energy structures for single charged silver clusters in the size of $Ag_n$ ($n = 21$–29). In the 45 structures of our figs, the handmade structures have occupied 20, including $Ag_{21}$**a**, $Ag_{21}^{+}$, $Ag_{22}$**a**, $Ag_{22}^{+}$, $Ag_{22}^{-}$, $Ag_{23}$**a**, $Ag_{23}^{+}$, $Ag_{23}^{-}$, $Ag_{24}$**a**, $Ag_{24}$**b**, $Ag_{25}$**a**, $Ag_{25}^{+}$, $Ag_{26}$**a**, $Ag_{26}^{-}$, $Ag_{27}$**a**, $Ag_{27}^{+}$, $Ag_{28}$**a**, $Ag_{28}^{-}$, $Ag_{29}$**a** and $Ag_{29}^{-}$. The symmetries and relative energies between the most stable structures and low-energy isomers are also listed.

The most stable structure of $Ag_{21}$, labeled as $Ag_{21}$**a** in Fig. 1, agrees with Itoh et al. [20]. $Ag_{21}$**b** is a 6–1–7–1–5 stacked structure with a capped atom in the top, whereas $Ag_{21}$**c** with a capped atom in the bottom. $Ag_{22}$**a** consists of an icosahedral core structure bonded to nine Ag atoms, which is 0.178 eV lower than the structure of Itoh et al. [20]. For $Ag_{23}$, the most stable structure $Ag_{23}$**a** with $C_{2v}$ symmetry can be regarded as adding one atom to the bottom of $Ag_{22}$**a**, which is found to be 0.572 eV smaller than the structure reported by Rogan et al. [30]. From $Ag_{24}$, the cluster starts to have a bulk-like stacking motif. The lowest-energy isomer $Ag_{24}$**a** is a 2–5–9–6–2 layer-stacking structure with $C_s$ symmetry. $Ag_{24}$**c** has 2–5–9–8 layered packing and exhibits $C_{2v}$ symmetry. For larger clusters, $Ag_{24}$**a** offers a good base for the formation of stable isomers of $Ag_{25-29}$. $Ag_{25}$**a** can be generated by adding one atom to the bottom of the $Ag_{24}$**a**. $Ag_{25}$**b** with $D_{3h}$ symmetry is stacked with 3–6–7–6–3 atoms on each layer. $Ag_{26}$**a** can be considered as adding a capped atom on the left edge of $Ag_{25}$**b**. $Ag_{26}$**b** can be viewed as adding an edge atom to the second layer of $Ag_{25}$**a**. Removing the capped atom of $Ag_{26}$**b** from its right side to the edge of central layer leads to another isomer $Ag_{26}$**c**. $Ag_{27}$**a** with $C_{2v}$ symmetry is stacked by taking away three capped atoms from the double-tetrahedral structure. $Ag_{27}$**b** is derived from adding a capped atom to the right of $Ag_{26}$**c** or a middle layer of $Ag_{26}$**b**. $Ag_{27}$**c** is stacked as 7–6–1–6–7 with $D_{6d}$ symmetry, which is the basic structure for $Ag_{28}$**a** and $Ag_{29}$**a**. For $Ag_{28}$**c**, each surface resembles a (1, 1, 1) surface stacked with 1–2–3–4 atoms or 2–3–4 atoms and is derived from adding a capped atom to the top of $Ag_{27}$**a**. $Ag_{29}$**b** can be considered as removing a capping atom from double-tetrahedron. $Ag_{29}$**c** stacked as 1–5–1–9–2–8–3 with $C_s$ symmetry as shown in Fig. 2.

From all neutral clusters mentioned above, we observed that $Ag_{21-23}$ grow with a 13-atom icosahedron or 19-atom double-icosahedron pattern. With size $n \geq 24$, $Ag_n$ ($n = 24$–27) prefer a bulk-like stacking and tend to form fcc (1, 1, 1) surfaces. The most stable structures for $Ag_{28}$ and $Ag_{29}$ are high symmetrical structures. Our calculation results show a different growth pattern of silver clusters with Shao' studies, which suggest that the domain motifs of $Ag_{21-29}$ are based on the distorted face-sharing icosahedra and fcc-like structure turn up for $Ag_n$ when $n = 38$ [18, 22].

### 3.2 Relative stabilities

Binding energies ($E_b$) per atom, second differences in energies ($\Delta^2 E$), and HOMO–LUMO gaps ($\Delta E_{H-L}$) were analyzed in our study to evaluate energetic stabilities of isomers. The corresponding values are listed in Table 1.

The binding energies per atom for neutral and single charged clusters are calculated as $E_b/n = (n\ E_1 - E_n)/n$ and $E_b/n = [(n-1)\ E_1 + E_1^{\pm} - E_n^{\pm}]/n$, respectively, where $E_n$ is the total energy of an $n$-atom cluster and $E_n^{\pm}$ is the total energy of a cationic and anionic $n$-atom cluster. Figure 3 depicts the binding energies per atom for the lowest-energy isomers of $Ag_n^v$ ($v = \pm 1, 0$; $n = 21$–29) as a function of cluster size. It can be seen from Fig. 3 that the binding energies per atom for both neutral and single charged $Ag_n$ increase gradually with the cluster size. Cationic clusters have the largest values among three types of clusters. Meanwhile, neutral clusters $Ag_n$ ($n = 22$, 24, 26, 29) have higher $E_b$ compared with related clusters. For single charged clusters, $Ag_n^+$ clusters with $n = 21$, 23, 25, 27 and $Ag_n^-$ clusters with $n = 23$, 25, 28, 29 show relatively high values of $E_b$. Note that $Ag_{24-29}$ are assembled as the double-tetrahedron structures, which are similar to the bulk crystal structures but with a stacking fault. The binding energies of these Ag clusters are about 74 % of the calculated binding energy (2.647 eV) of bulk Ag (lattice constant $a_0 = 4.0857$ Å). It appears that the double-tetrahedron motif would be a preferred growth pattern for the medium-sized silver clusters. Second differences in energies is defined by $\Delta^2 E_n^v = E_{n+1}^v + E_{n-1}^v - 2\,E_n^v$, where $E_{n+1}^v$, $E_{n-1}^v$ and $E_n^v$ are the total energies of the lowest-energy structures of $Ag_{n+1}^v$, $Ag_{n-1}^v$ and $Ag_n^v$, respectively. As seen in Table 1, second differences in energies of neutral and cationic clusters exhibit significantly odd–even alternations. Second differences in energies are larger at neutral clusters $Ag_{22}$, $Ag_{24}$, $Ag_{26}$ and charged clusters $Ag_{23}^+$, $Ag_{25}^+$, $Ag_{27}^+$, and $Ag_{23}^-$, $Ag_{25}^-$ and $Ag_{28}^-$. Thus, these clusters are more favorable in energies than their neighboring clusters.

### 3.3 Ionization potentials and electronic affinities

The ionization potentials (IPs) and electronic affinities (EAs) for the lowest-energy structures of $Ag_n$ ($n = 4$–29) as a function of cluster size are described in Figs. 6 and 7. For $n \leq 20$, we repeated and calculated all the lowest-energy

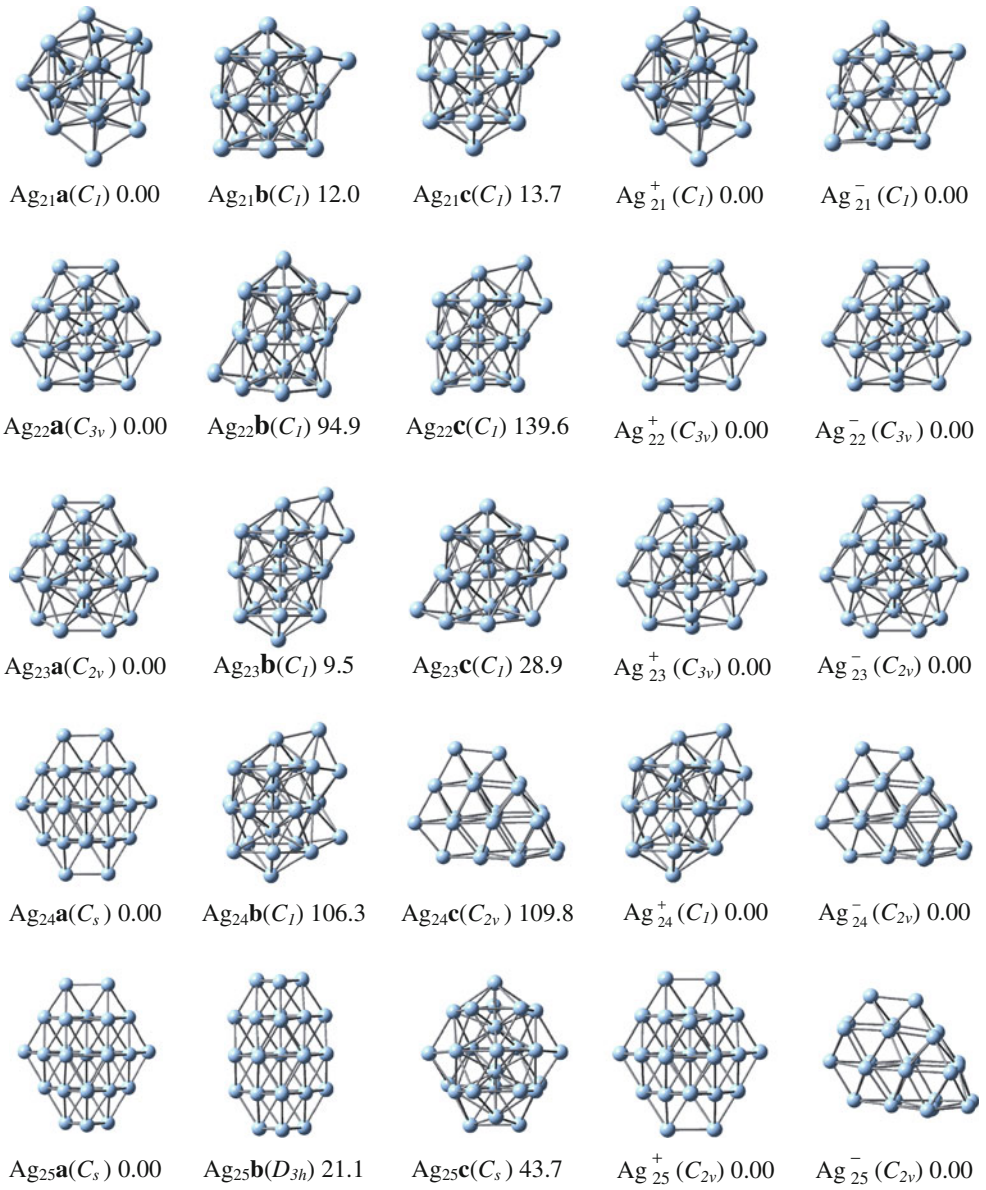


**Fig. 1** Three low-energy isomers (**a**, **b**, **c**) of neutral $Ag_n$ ($n = 21$–25) and the lowest-energy structures of cationic and anionic $Ag_n$. Relative energies (meV) were calculated at the PW91/DNP level

structures of silver clusters from the literature [20] with DFT method. Combined with our structures presented in this paper, we extend the size of silver cluster in the IPs and EAs calculations up to 29 atoms.

The IP is defined as a straightforward difference in the total energies of the neutral and charged clusters, without or with the relaxations of the charged cluster structures to evaluate the vertical or adiabatic IP, respectively. The EA is defined as following: $EA = E_n - E^{-}_{n}$, where $E^{-}_{n}$ is the total energy of the optimal $Ag_n^-$ for adiabatic electron affinity (AEA). The whole tendency of the adiabatic IPs we calculated in Fig. 4 agrees well with the result of the photoionization spectroscopy measurement [31], though the calculated AIP are lower $0.3 - 1.3$ eV than the experimental data. Strong oscillating behavior is displayed by higher IP values for clusters with even number atoms, indicating that odd-atom clusters are apt to lose an electron to keep stable. In Fig. 4, 10 apparent peaks at $Ag_n$ ($n = 6$, 8, 12, 14, 18, 20, 22, 24, 26, 28) can be found, which correspond to the complete structural motifs or the "magic number" clusters. Particularly, $Ag_6$, $Ag_8$ and $Ag_{14}$ have larger IP values, which are predicted to be the "magic number" clusters in the literature [13]. In more detail, from $Ag_{21}$ to $Ag_{29}$, sharp increases in IPs occur from $n = 21$ to 22, 23 to 24 and 27 to 28 as results of structural evolution from icosahedral and double-icosahedral structures to fcc-based structures to structures with a disclination axis.

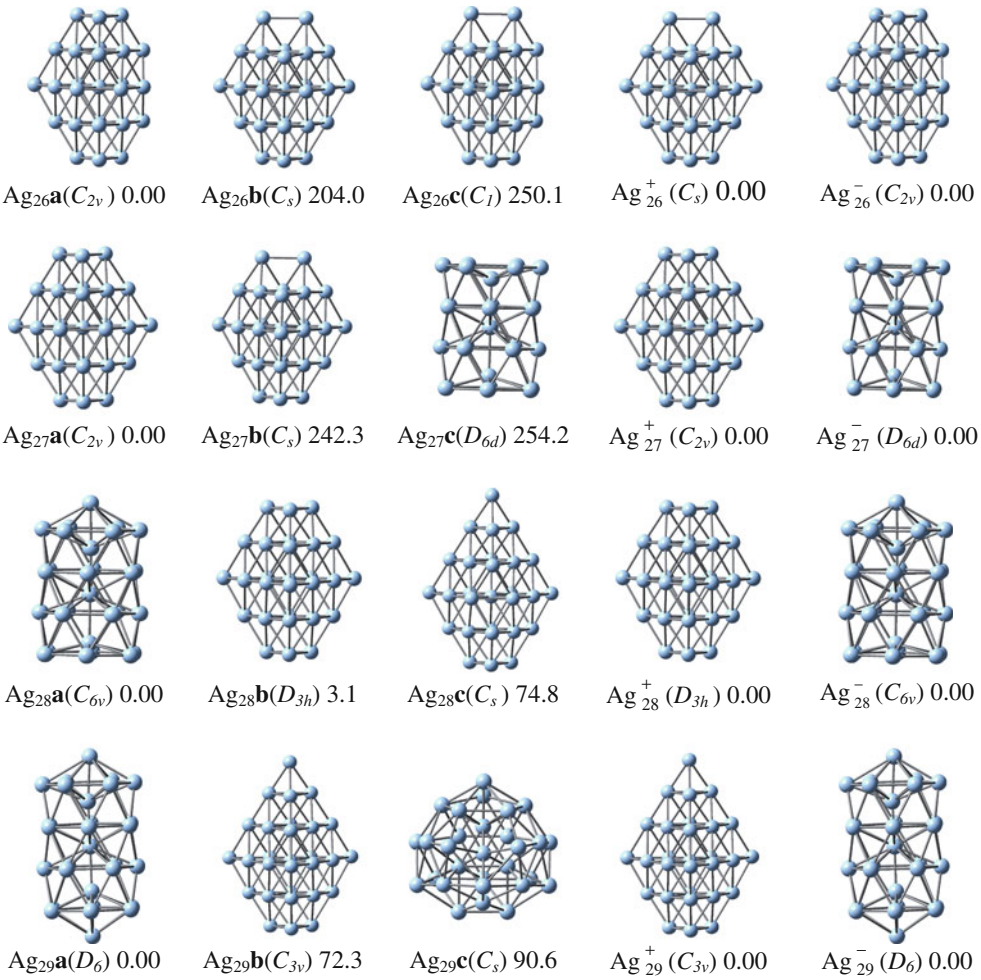


**Fig. 2** Three low-energy isomers (**a**, **b**, **c**) of neutral $Ag_n$ ($n = 26$–29) and the lowest-energy structures of cationic and anionic $Ag_n$. Relative energies (meV) were calculated at the PW91/DNP level

**Table 1** Binding energies per atom, second differences in energies and HOMO–LUMO gaps of $Ag_n^v$ ($v = \pm1, 0$; $n = 21$–29) clusters

| | $E_b$ (eV) | | | $\Delta^2E$ (eV) | | | $\Delta H$–$L$ (eV) | | |
|---|---|---|---|---|---|---|---|---|---|
| | Cationic | Neutral | Anionic | Cationic | Neutral | Anionic | Cationic | Neutral | Anionic |
| $Ag_{21}$ | 2.0390 | 1.8867 | 1.9671 | – | – | – | 1.0427 | 0.1218 | 0.5645 |
| $Ag_{22}$ | 2.0331 | 1.9038 | 1.9707 | −0.2111 | 0.3627 | −0.1780 | 0.0978 | 0.5479 | 0.6047 |
| $Ag_{23}$ | 2.0368 | 1.9036 | 1.9823 | 0.1609 | −0.4119 | 0.1272 | 0.8309 | 0.0960 | 0.6918 |
| $Ag_{24}$ | 2.0336 | 1.9206 | 1.9877 | −0.5443 | 0.2545 | −0.3184 | 0.0999 | 0.9065 | 0.0973 |
| $Ag_{25}$ | 2.0524 | 1.9261 | 2.0054 | 0.4226 | −0.4319 | 0.3431 | 1.2234 | 0.0950 | 0.8081 |
| $Ag_{26}$ | 2.0534 | 1.9478 | 2.0085 | −0.4551 | 0.4129 | −0.2284 | 0.1031 | 0.8716 | 0.8461 |
| $Ag_{27}$ | 2.0713 | 1.9526 | 2.0198 | 0.4365 | −0.0218 | −0.0030 | 0.8648 | 0.7652 | 0.1777 |
| $Ag_{28}$ | 2.0723 | 1.9578 | 2.0305 | 0.0946 | 0.0367 | 0.2141 | 1.1885 | 0.2485 | 0.0626 |
| $Ag_{29}$ | 2.0699 | 1.9613 | 2.0330 | – | – | – | 0.7035 | 0.6391 | 0.6563 |

The calculated EA is described in Fig. 5, which is compared with ultraviolet photoelectron spectra data and predicted EA values in shell model with ab initio calculations [32]. It is obvious that the calculated EA values in this study exhibit similar trend with the UPS data except for the deviation from $Ag_{16–17}$ and $Ag_{21–22}$. In Fig. 5, the "magic number" cluster $Ag_8$ has the lowest value of EA due to its special stability. However, $Ag_{29}$ with the highest value of EA is considered to be easier to get an electron than its neighboring clusters. For $n = 21$–29, $Ag_n$ clusters at special values of $n = 22, 24, 26$ have valleys of EA, which reflects the relative electronic stabilities of these clusters.

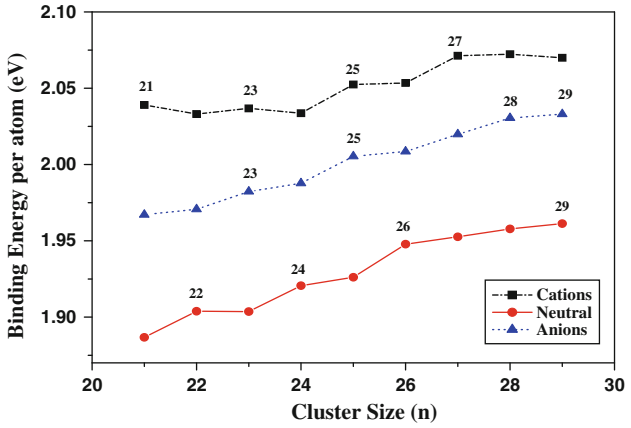


**Fig. 3** Binding energies per atom for the lowest-energy structures of cationic, neutral and anionic clusters of $Ag_n$ ($n = 21$–29) versus cluster size

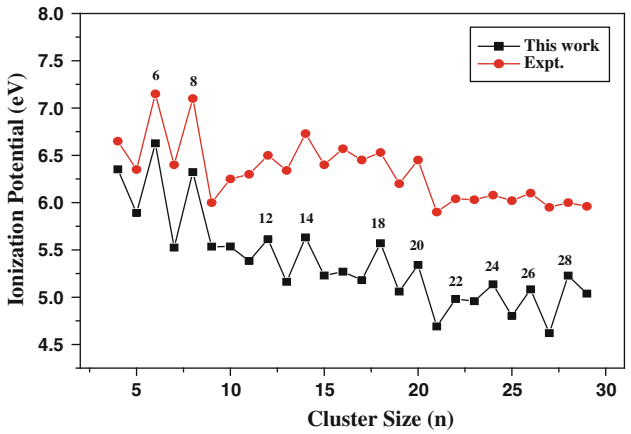


**Fig. 4** Calculated IPs versus cluster size for $Ag_n$ ($n = 4$–29) compared with the photoionization experiment [31]

### 3.4 Optical absorption spectra

We calculated the absorption spectra for medium-sized $Ag_n$ ($n = 21$–29) clusters, which are compared to existing experimental data ($Ag_{21}$, $Ag_{23}$, $Ag_{25}$ and $Ag_{27}$). The TDDFT calculated optical absorption spectra for $Ag_n$ ($n = 21$–29) along with experimental spectra [33–35] are plotted in Fig. 6. Note that for $Ag_{21}$, the spectra were only calculated in the 2.5–5.1 eV range. The experimental spectra are characterized by the emergence of a dominant and relatively broad peak between 3.2 and 4.2 eV, accompanied by one or two absorption peaks at higher energies (Fig. 6). The common feature is following a slight blueshift of the main peak with increasing cluster size. The calculated spectra are generally in good agreement with the experimental ones.

For $Ag_{21}$ (Fig. 6), the absorption spectra were obtained by Fedrigo et al. [33] in an Ar matrix at 28 K. It shows two main peaks at 3.56 and 3.74 eV. Our calculated spectra for

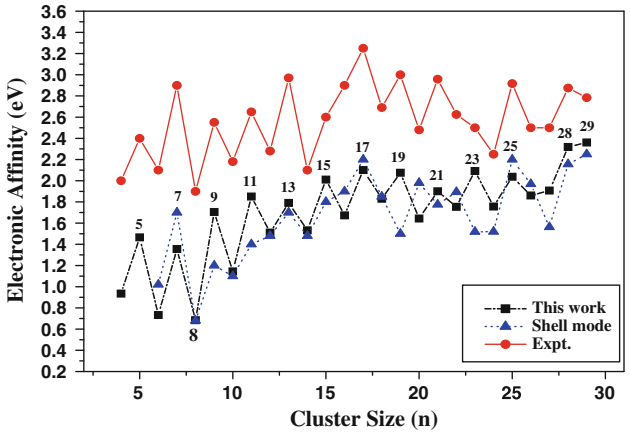


**Fig. 5** Calculated EAs for $Ag_n$ ($n = 4$–29) versus cluster size compared with shell model calculated results and experimental EAs data [32]

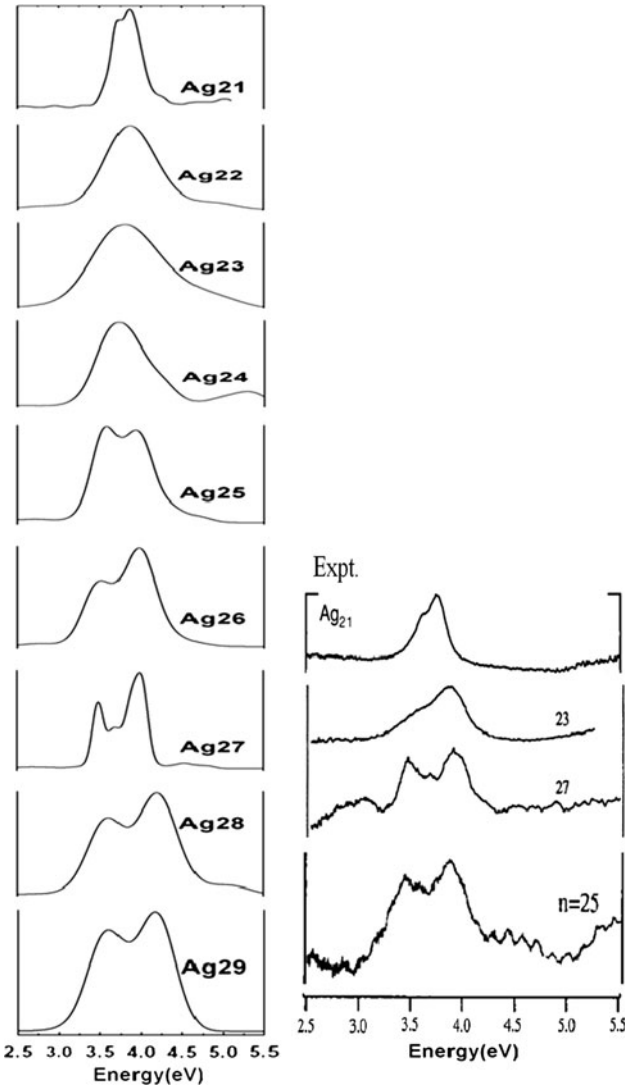


**Fig. 6** TDDFT calculated absorption spectra for Ag 21–29. The experimental spectra from Fedrigo et al. [33] (Ag 21), [34] (Ag 23 and 27) and [35] (Ag 25)

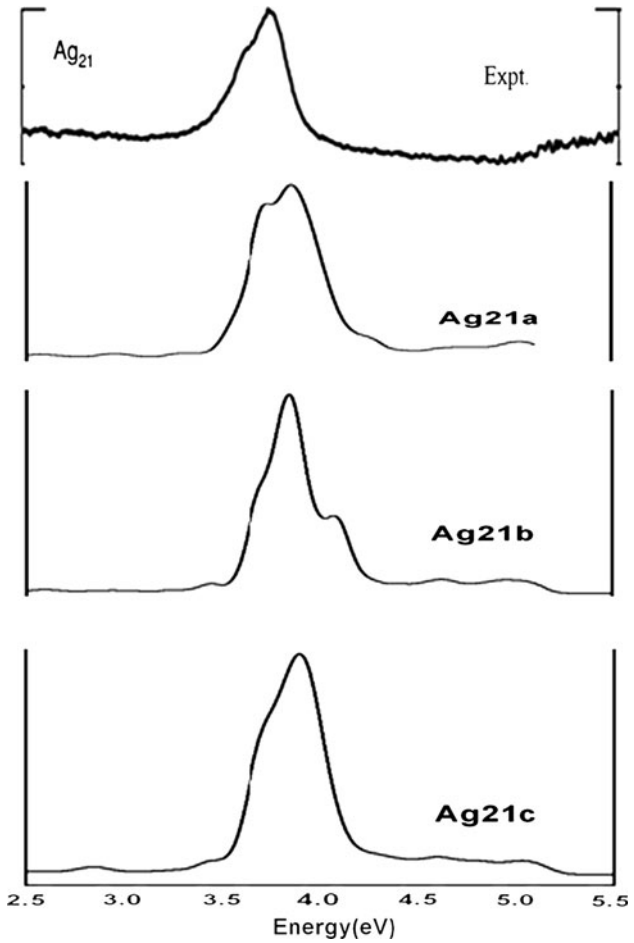


**Fig. 7** The experimental and TDDFT calculated absorption spectra for three different isomers of $Ag_{21}$

the lowest-energy structure of $Ag_{21}$ predict well the shape of the experimental one. In particular, the second main peak of the spectrum presents at 3.75 eV is in good agreement with the second peak of the experimental spectrum at 3.74 eV. The first peak of the spectrum at 3.56 eV is blueshifted with respect to the experiment by about 0.13 eV. For $Ag_{23}$, the spectra of the lowest-energy structure give a main peak at 3.86 eV followed with a broad peak, in very good agreement with the experimental spectrum [34]. The experimental spectrum of $Ag_{25}$ shows two main peaks at 3.42 and 3.87 eV [35]. Spectra of the lowest-energy isomer have very similar shapes with two main peaks at similar energies and broad. Finally, the experimental spectrum of $Ag_{27}$ consists of two main peaks at 3.41 and 3.90 eV [34]. Comparing this spectrum with the lowest-energy isomer, we observe that the overall shape is best matched by the spectrum, which exhibits the main peak at 3.48 and 3.90 eV.

For further certificating the confidence of the lowest-energy isomers, we also calculated the absorption spectra of some other isomers. Different isomers can give different optical spectra. For example, the absorption spectra of three different isomers of $Ag_{21}$ are shown in Fig. 7. Our calculated spectra for the lowest-energy structures $Ag_{21}$a are generally in good agreement with the experimental ones and are good matched shapes of the experimental spectrum.

## 4 Conclusion

The lowest-energy structures of $Ag_n^v$ ($v = \pm 1, 0$; $n = 21$–$29$) were predicted theoretically. Among the lowest-energy structures of these medium-sized silver clusters, the ground-state geometries for $Ag_{21-23}$ prefer icosahedral or double-icosahedral core structures. When the cluster size reaches 24, the most stable structure motif apparently differs from the $Ag_{21-23}$ series, which has a tendency to grow in a bulk-like fcc stacking. The lowest-energy structures of $Ag_{28}$ and $Ag_{29}$ display another new structural frame. It means that medium-sized silver clusters have a competition between icosahedral, bulk-like fcc and disordered structures. Analysis of the relative stabilities, the IPs and EAs suggests that neutral clusters $Ag_{22}$, $Ag_{24}$, $Ag_{26}$, cationic clusters $Ag_{21}^+$, $Ag_{23}^+$, $Ag_{25}^+$ and anionic clusters $Ag_{23}^-$, $Ag_{25}^-$ display relative larger energetic, chemical and electronic stabilities. Besides, the behaviors of the calculated IPs and EAs of $Ag_n$ ($n = 4$–$29$) are also in agreement with the experimental results. And the calculated spectra are generally in good agreement with the experimental ones and are good matched shapes of the experimental spectrum.

**Acknowledgments** This work was supported by the National Natural Science Foundation of China (Nos. 20973076, 21173096 and 21043001) and Specialized Research Fund for the Doctoral Program of Higher Education (20110061110018). This work was also supported by Jilin Province Science and Technology Development Plan (No. 201101063).

## References

1. Eachus RS, Marchetti AP, Muenter AA (1999) Annu Rev Phys Chem 50:117
2. Koretsky GM, Knickelbein MB (1997) J Chem Phys 107:10555
3. Kim SH, Medeiros-Ribeiro G, Ohlberg DAA, Williams RS, Heath JR (1999) J Phys Chem B 103:10341
4. Chan WT, Fournier R (1999) Chem Phys Lett 315:257
5. Lee I, Han SW, Kim K (2001) Chem Commun 18:1782
6. Johnston RL (2003) Dalton Trans 2003:4193
7. Ziella DH, Caputo MC, Provasi PF (2011) Int J Quantum Chem 111:1680
8. Neogrády P, Kellö V, Urban M, Sadlej AJ (1997) Int J Quantum Chem 63:557
9. Dong Y, Springborg M, Warnke I (2011) Theor Chem Acc 130:1001
10. Weis P, Bierweiler T, Gilb S, Kappes MM (2002) Chem Phys Lett 355:355

11. Huda MN, Ray AK (2003) Phys Rev A 67:013201
12. Fournier R (2001) J Chem Phys 115:2165
13. Zhang HL, Tian DX (2008) Comput Mater Sci 42:462
14. Harb M, Rabilloud F, Simon D, Rydlo A, Lecoultre S, Conus F, Rodrigues V, Félix C (2008) J Chem Phys 129:194108
15. Baishya K, Idrobo JC, Öğüt S, Yang ML, Jackson K, Jellinek J (2008) Phys Rev B 78:075439
16. Wang JL, Wang GH, Zhao JJ (2003) Chem Phys Lett 380:716
17. Michaelian K, Rendón N, Garzón IL (1999) Phys Rev B 60:2000
18. Shao XG, Liu XM, Cai WS (2005) J Chem Theory Comput 1:762
19. Zhao J, Luo Y, Wang G (2001) Eur Phys J D 14:309
20. Itoh M, Kumar V, Adschiri T, Kawazoe Y (2009) J Chem Phys 131:174510
21. Häkkinen H, Moseler M, Kostko O, Morgner N, Hoffmann MA, Issendorff BV (2004) Phys Rev Lett 93:093401
22. Yang XL, Cai WS, Shao XG (2007) J Phys Chem A 111:5048
23. Peterson MR, Doom TE, Raymer ML (2004) Lect Notes Comput Sci 3102:426
24. Zhang W, Lu WC, Sun J, Wang CZ, Ho KM (2008) Chem Phys Lett 455:232
25. Zhang W, Lu WC, Zang QJ, Wang CZ, Ho KM (2009) J Chem Phys 130:144701
26. Delley B (1990) J Chem Phys 92:508
27. Delley B (2000) J Chem Phys 113:7756
28. Perdew JP, Chevary JA, Vosko SH, Jackson KA, Pederson MR, Singh DJ, Fiolhais C (1992) Phys Rev B 46:6671
29. Koelling DD, Harmon BN (1997) J Phys C Solid State Phys 10:3107
30. Rogan J, Ramírez M, Muñoz V, Valdivia JA, García G, Ramírez R, Kiwi M (2009) J Phys Condens Matter 21:084209
31. Jackschath C, Rabin I, Schulze W (1992) Z Phys D-Atoms Mol Clust 22:517
32. Taylor KJ, Pettiette-Hall CL, Cheshnovsky O, Smalley RE (1992) J Chem Phys 96:3319
33. Fedrigo S, Harbich W, Buttet J (1993) Phys Rev B 47:10706
34. Harbich W, Fedrtgo S, Buttet J (1993) Z Phys D-Atoms Mol Clust 26:138
35. Fedrigo S, Harbich W, Belyaev J, Buttet J (1993) Chem Phys Lett 211:166